Organic Geochemistry 58 (2013) 115–120

Contents lists available at SciVerse ScienceDirect

Organic Geochemistry

journal homepage: www.elsevier.com/locate/orggeochem

Alkenone and tetraether lipids reflect different seasonal seawater temperatures in the coastal northern South China Sea

Jie Zhang [a,b], Yang Bai [a], Shendong Xu [a], Fei Lei [a], Guodong Jia [a,*]

[a] CAS Key Laboratory of Marginal Sea Geology, Guangzhou Institute of Geochemistry, Chinese Academy of Sciences, Guangzhou 510640, China
[b] Zibo Environmental Monitoring Station, Zibo 255000, China

ARTICLE INFO

Article history:
Received 1 October 2012
Received in revised form 17 February 2013
Accepted 19 February 2013
Available online 13 March 2013

ABSTRACT

We examined the lipid-based temperature proxies $U^{K'}_{37}$ and TEX^{H}_{86} in five short sediment cores from the inner shelf of the northern South China Sea and related them to local sea water temperature from the World Ocean Atlas (WOA) database. The $U^{K'}_{37}$-based temperature values are consistent with euphotic zone temperature in spring and summer, when the southeast monsoon prevails and vertical stratification occurs in the water column, whereas TEX^{H}_{86}-based temperature values reflect sea surface temperature in winter when the northeast monsoon prevails and vertical mixing occurs. The different temperature signals between the TEX^{H}_{86} and $U^{K'}_{37}$ proxies could be a result of differences in the growing season between the source organisms, with alkenone-producing haptophyte algae blooming in the warmer and nutrient-rich season with higher fluvial influx, and tetraether-producing Thaumarchaeota blooming in the cooler and oligotrophic season.

1. Introduction

$U^{K'}_{37}$ and TEX_{86} are seawater temperature proxies based on haptophyte-produced alkenones and Thaumarchaeota-produced glycerol dialkyl glycerol tetraethers (GDGTs), respectively (Prahl and Wakeham, 1987; Schouten et al., 2002). Generally, they are accepted as indicators of annual mean sea surface temperature (SST), and have been widely used for paleo-SST reconstruction (reviewed by Schouten et al., 2013). However, paired analysis of $U^{K'}_{37}$ and TEX_{86} proxies in core top and downcore sediments in some regions has revealed that temperature values based on the two proxies tend to be different, and hence have different meanings. For example, in the offshore Adriatic Sea and the Eastern Mediterranean TEX_{86}-based temperature values were higher than $U^{K'}_{37}$-based values, likely due to seasonal differences between the timing of the haptophyte (winter) and Thaumarchaeota (summer) blooms (Castañeda et al., 2010; Leider et al., 2010). Thaumarchaeota can also bloom during winter, thereby giving cold-biased TEX_{86} temperature values, as observed in the North Sea (Herfort et al., 2006). Other studies have shown that in some settings TEX_{86}-based temperature values are lower than corresponding $U^{K'}_{37}$-based values, suggestive of a subsurface water signal recorded by TEX_{86}, for example, in the Santa Barbara Basin (Huguet et al., 2007), the Benguela upwelling area (Lee et al., 2008) and the west coast of Africa (Lopes dos Santos et al., 2010). These results therefore highlight the importance of performing calibration studies using sediment traps and core tops before applying the temperature proxies in a given study area.

The South China Sea (SCS) is a large marginal sea in the tropical western Pacific and affords archives of high quality sediment for paleoceanographic research. A recent study suggests that the TEX_{86} record in the SCS may be consistent with annual sea surface temperature (SST) in the open sea (Wei et al., 2011; Ge et al., 2013). However, Jia et al. (2012) showed that the TEX_{86}- and $U^{K'}_{37}$-based temperature values for deep water (>300 m) core top sediments in the SCS may record subsurface, specifically 30–125 m, water temperature and SST, respectively. On the shallow inner shelf of the northern SCS, Wei et al. (2011) and Ge et al. (2013) showed significantly lower sedimentary TEX_{86} temperature estimates than the mean annual SST based on satellite data. In Wei et al. (2011), no specific reason was given for the low TEX_{86} values, whereas the Ge et al. (2013) study realized that TEX_{86} might reflect winter temperature. However, there is a lack of an integrated study of $U^{K'}_{37}$ and TEX_{86} in this region. Here, we show that, unlike in the open SCS, the two proxies reflect different seasonal seawater temperatures in this coastal area.

2. Material and methods

2.1. Study area and sample collection

The northern coastal SCS off the Pearl River estuary (PRE; Fig. 1) is characterized by a tropical and subtropical monsoon climate and complex hydrological environments. Wind speed of the NE monsoon is much stronger in winter than that of the SW monsoon in

* Corresponding author. Tel.: +86 20 85290157; fax: +86 20 85290278.
E-mail address: jiagd@gig.ac.cn (G. Jia).

0146-6380/$ - see front matter © 2013 Elsevier Ltd. All rights reserved.
http://dx.doi.org/10.1016/j.orggeochem.2013.02.012

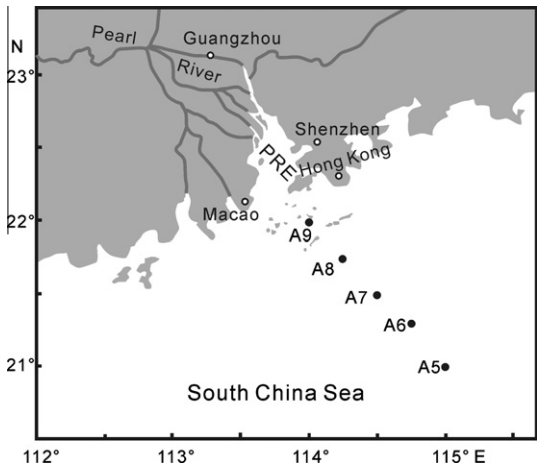

Fig. 1. Location of sediment cores from the coastal northern SCS (PRE, Pearl River Estuary).

summer in the area. In response to the seasonal changing directions of the East Asian monsoon, the coastal current flows northeastward in summer and reverses direction in winter (Su, 2004). The outflow of the PR also greatly influences coastal water, mostly in the wet season, by delivering large amounts of nutrients (Zhai et al., 2005). Water column temperature in the study area displays an annual cycle, showing vertical stratification and horizontal homogenization in the warm and wet season, and strong vertical mixing and an inshore–offshore temperature gradient in the cool and dry season (Fig. 2).

Productivity in the coastal area is linked to nutrient load in the photic zone, which is significantly controlled by fluvial input. The PR discharge, as well as nutrient influx, is characterized by peak flooding during summer, which can induce a large phytoplankton bloom (Dai et al., 2008). In the dry winter, although vertical mixing occurs, nutrient level falls because of the combined effects of lower terrestrial nutrient input, near-shore downwelling (Liu et al., 2010) and the oligotrophic nature of the SCS surface water. Primary productivity was reported to be an order of magnitude higher in summer (433.2 mg C m^{-2} d^{-1}; Song et al., 2010) than in winter (41.3 mg C m^{-2} d^{-1}; Le et al., 2008). Diatoms are predominant in the phytoplankton both in winter and summer, with coccolithophores, mainly *Emiliania huxleyi*, remaining minor but common in the area (Le et al., 2006; Sun et al., 2007). Detailed phytoplankton dynamics have yet to be investigated. Little is known about Thaumarchaeota in the area, although they may be ubiquitous and abundant in coastal waters (e.g. Urakawa et al., 2010).

Five box cores A5 to A9 (Table 1) were collected during the China Ocean Carbon (CHOICE-C) Cruise I onboard the Dongfanghong II in August 2009. They were from along a cross-shelf transect off the PRE and Hong Kong to the southeast in the inner shelf of the northern SCS (Fig. 1). Core A9 was located inshore near the PRE mouth and A5 from offshore at the distal end. The core tops were well preserved upon collection, as evidenced by fairly clear water above the sediment in the box corer. After the overlying water was siphoned off, core barrels (11.4 cm i.d.; 60 cm length) were pushed into the box to obtain sub-cores. Sediments in the sub-cores were (usually within 1 h) extruded onboard with a hydraulic jack and sectioned at 2 cm intervals. The sectioned samples were sealed in plastic jars (8.5 cm i.d.; 7.5 cm height) and kept frozen until analysis in the laboratory.

In addition, we collected 2 soil samples on land, and 3 sediment samples and 2 suspended matter samples from the main river channel upstream of the PRE.

2.2. Analytical methods

All five cores were dated using ^{210}Pb methods and the results shown in Table 1 have been discussed elsewhere (Lei et al., 2012; Jia et al., in press). The freeze-dried samples were ultrasonically extracted. For the purification of extract, column chromatography and instrumental analysis of GDGTs and alkenones we referred to Hopmans et al. (2000) and Villanueva et al. (1997), respectively, and the details are described by Jia et al. (2012). $U^{K'}_{37}$ and TEX_{86} values were calculated on the basis of established equations (Prahl and Wakeham, 1987; Schouten et al., 2002). As the calibration of TEX_{86} has been updated several times (reviewed by Schouten et al. (2013)), we applied the most up to date global calibration by Kim et al. (2010) for temperature estimation:

$$T = 68.4 \times (TEX^{H}_{86}) + 38.6 \quad (r^2\ 0.87, n = 255)$$

where $TEX^{H}_{86} = \log(TEX_{86})$. $U^{K'}_{37}$-based temperature was calculated using the global calibration of Müller et al. (1998):

$$T = (U^{K'}_{37} - 0.044)/0.033) \quad (r^2\ 0.958, n = 370)$$

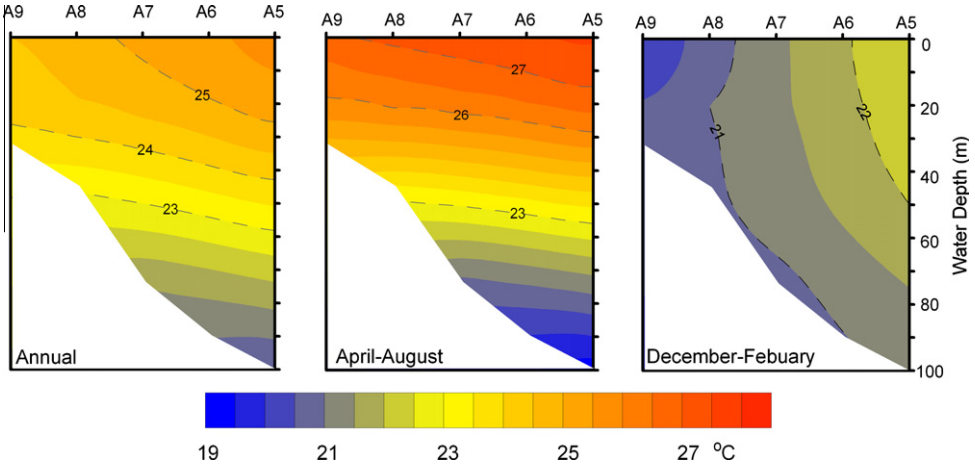

Fig. 2. Sea water temperature distributions during different time periods in the study area. Temperature data were downloaded online from the World Ocean Atlas (WOA) 2001 in the National Oceanographic Data Center (NODC) on a 1/4° grid resolution (http://www.nodc.noaa.gov/OC5/WOA01/qd_ts01.html).

Table 1
Information on sediment cores and ^{210}Pb dating results.

	A5	A6	A7	A8	A9
Location					
Latitude (N)	21.0	21.25	21.5	21.8	22.0
Longtitude (E)	115.0	114.7	114.5	114.2	114.0
Water depth (m)	102	89	73	45	33
Core length (cm)	24	34	20	48	52
Dating model (CIC)					
MAR (g cm^{-2} yr^{-1})[a]	0.28	0.33	0.16	0.35	0.48
Time span (yr)	1901–2006	1902–2008	1906–2006	1892–2008	1936–2008
MTR[b] per 2 cm interval (yr)	9.6	6.6	11.1	2.4	3.3

[a] Mass accumulation rate.
[b] Mean temporal resolution.

2.3. Temperature in the water column

Temperature data for every core location were downloaded online from the World Ocean Atlas (WOA) 2001 in the National Oceanographic Data Center (NODC) on a 1/4° grid resolution (http://www.nodc.noaa.gov/OC5/WOA01/qd_ts01.html). The database provides 3 D interpolation onto 24 standardized vertical intervals from the surface (0 m) to the seafloor (5500 m) for monthly mean parameters.

3. Results and discussion

3.1. TEX_{86}^{H} and $U_{37}^{K'}$ derived temperatures

A key difficulty for using TEX_{86} estimates in marine environment is the contribution from isoprenoid GDGTs of continental origin (Weijers et al., 2006), which should be given special attention in large river-influenced coastal areas. The BIT index, a proxy based on the relative abundance of soil derived branched tetraether lipids vs. crenarchaeol for estimating the relative contribution of soil organic matter (OM) to marine sediments (Hopmans et al., 2004; Weijers et al., 2006), exhibits values between 0.90 and 0.99 in our soil and river samples upstream of the PRE. In the PRE, BIT decreases from >0.9 in the sediments at the freshwater entrance to <0.4 at the PRE mouth (Strong et al., 2012; Zhang et al., 2012), suggestive of a reducing soil OM contribution along the flow path from terrestrial to marine environments. For our cores, BIT values are 0.20 ± 0.03, 0.22 ± 0.03, 0.17 ± 0.02, 0.13 ± 0.02 and 0.12 ± 0.01 in cores A9, A8, A7, A6 and A5, respectively, exhibiting a slightly shoreward increasing trend. This BIT pattern fits with the expected shoreward increasing contribution of soil OM; however, all BIT values (range 0.09–0.27) are within the range for marine sediments used for TEX_{86}^{H} calibration (e.g. Kim et al., 2010), reflecting minor influence of soil-derived GDGTs on the use of TEX_{86}^{H} as a sea water temperature proxy. This point is further discussed below.

GDGT data from core tops of A5, A7 and A9 have been analyzed in another lab and published elsewhere (Wei et al., 2011), showing TEX_{86}^{H}-based temperatures of 23.2 °C, 20.4 °C and 18.4 °C, respectively, for the three sites. Similarly, our downcore mean temperature values estimated from TEX_{86}^{H} are 23.3 ± 0.9 °C (range 21.7–24.5 °C), 22.3 ± 0.8 °C (range 20.7–23.5 °C), 21.2 ± 1.0 °C (range 19.8–23.0 °C), 20.7 ± 0.5 °C (range 19.7–21.8 °C), 18.1 ± 1.3 °C (range 15.6–21.4 °C) in A5, A6, A7, A8 and A9, respectively (Figs. 3 and 4). This shoreward cooling trend is similar to the BIT distribution, which exhibits increasing values from A5 to A9, implying that soil derived isoprenoid GDGTs in sediments might have caused the TEX_{86}^{H} derived temperature pattern. However, the TEX_{86}^{H} "temperature" in soils, river sediments and suspended matter from the PR delta ranges from 20.2 to 26.6 °C, with a mean value of 23.3 ± 2.1 °C, too high to be responsible for the observed shoreward cooling trend. So, soil derived GDGTs are unlikely to be the cause of the observed TEX_{86}^{H} temperature distribution.

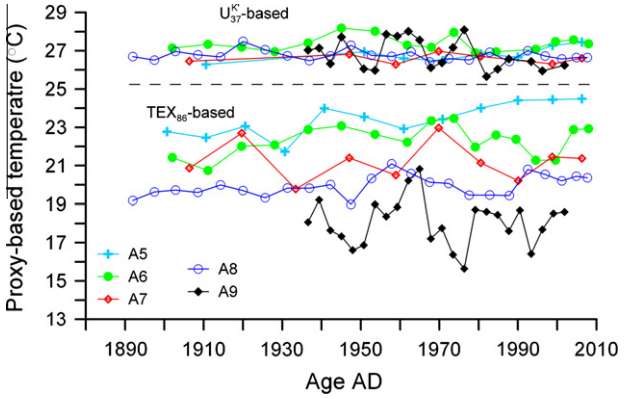

Fig. 3. Downcore temperature in the five cores based on $U_{37}^{K'}$ and TEX_{86} proxies.

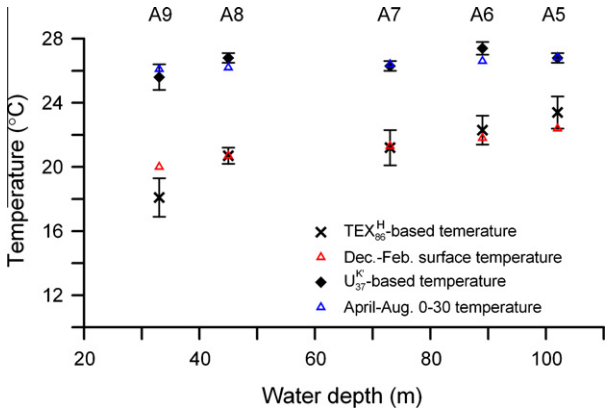

Fig. 4. Comparison of downcore mean $U_{37}^{K'}$- and TEX_{86}-based temperatures, respectively, with WOA seasonal water temperatures at the five sites.

We also noticed that the above estimated temperature values are lower than the corresponding WOA annual temperature values at any water depth between 0 and 40 m (Fig. 2), suggesting that TEX_{86}^{H} derived values do not reflect annual SST in the study area. Given that Thaumarchaeota can grow chemolithoautotrophically by aerobically oxidizing NH_3 to NO_2^- in deeper water and low reconstructed temperature values could result from subsurface production of GDGTs [reviewed by Schouten et al. (2013)], our TEX_{86}^{H} derived values could likely reflect subsurface temperature. However, employing the calibration of TEX_{86}^{H} vs. 0–200 m water temperature (i.e. $T = 54.7 \times TEX_{86}^{H} + 30.7$) proposed by Kim et al. (2012), which contains subsurface temperature signals and is

actually identical to the calibration for 30–125 m water temperature in the open SCS (Jia et al., 2012), would result in unrealistic values lower than bottom temperature. Additionally, the horizontal WOA annual temperature gradient (<1 °C) throughout the water column is much smaller than the gradient from our TEX_{86}^{H} estimates (>5 °C). Therefore, invoking a substantial contribution of GDGTs from subsurface appears not suitable for this shallow (33–102 m) coastal area.

On the other hand, the shoreward cooling trend in TEX_{86}^{H}-derived temperature is similar to the winter SST pattern shown in Fig. 2, and the corresponding WOA-derived winter SST for these sites is: 22.3 °C (A5), 21.8 °C (A6), 21.3 °C (A7), 20.6 °C (A8) and 19.7 °C (A9). Apparently, the differences between the TEX_{86}^{H}-based temperature and WOA derived winter SST are within 1 °C except at site A9, where it reaches 1.6 °C (Fig. 4). Similarly, using the TEX_{86} calibration proposed by Kim et al. (2008) also resulted in temperature differences <1 °C, except 2.3 °C at A9. The larger difference at A9 is not clear at present, but might be related to some local temperature variation, as discussed below, that is not captured in WOA. Nevertheless, the above differences are well within the estimation error of 2.5 °C from the TEX_{86}^{H} calibration (Kim et al., 2010), so the general agreement between TEX_{86}^{H} temperature and WOA winter SST demonstrates that TEX_{86}^{H} derived temperature mainly reflects winter temperature in the study area.

While GDGTs are abundant throughout the cores, in some samples long chain alkenones are either not present or are below detection limit. Unlike TEX_{86}^{H} temperature, downcore mean $U_{37}^{K'}$-based temperature values for the five cores (25.6–27.4 °C) are higher than the corresponding WOA annual SST (24.5–25.7 °C), but lower than summer SST (>28 °C). Additionally, there is only a small shoreward cooling trend (<0.8 °C) in the $U_{37}^{K'}$ temperature signal. We therefore explored the season and/or water depth from which the temperature signals appear to be derived by comparing the mean $U_{37}^{K'}$-based values with the mean WOA values at varying water column depth (WCD) and monthly intervals. Minimum differences (−0.5 to +0.8 °C) between $U_{37}^{K'}$-based values and WOA values were observed for two scenarios: (i) at 0–30 m WCD from April to August (Fig. 4) and (ii) at the sea surface (i.e. 0 m WCD) from March to November. Since alkenone-producing haptophytes live in the euphotic zone rather than only at the surface, we prefer the former scenario as the determinant of the $U_{37}^{K'}$ temperature signal. This suggests that the $U_{37}^{K'}$ proxy indicates the spring and summer upper layer water temperature in the study area. Time series curves of $U_{37}^{K'}$-based temperature do not show offset between the five cores (Fig. 3). This is in agreement with the horizontal temperature homogenization in the warm season, confirming that the $U_{37}^{K'}$ proxy reflects the warm season temperature signal.

Unlike $U_{37}^{K'}$-based temperature curves, time series TEX_{86}^{H}-based temperature estimates from the five cores exhibit a general shoreward cooling trend (Fig. 3), similar to the winter temperature distribution. However, temperature variation based on TEX_{86}^{H} does not appear to agree well between cores. This might be due to several possible factors pending further research, for example, the different density and time resolution of data points for these records, age model uncertainty, and sediment winnowing and focusing associated with seabed morphology or water circulation. In addition, we note that the variability in both $U_{37}^{K'}$ and TEX_{86}^{H} derived temperature is greater for core A9 than the other cores (Fig. 3). This might be associated with the proximity of site A9 to the PRE mouth, which makes the local sea water temperature prone to be influenced by river water input that is quite variable in temperature and discharge. However, given the low and usually southwestward fluvial discharge during winter, the large temporal variation (up to 5.2 °C) for TEX_{86}^{H} derived temperature in core A9 seems not likely caused solely by the interference of river water. Recently, Liu et al. (2010) reported from an in situ observation in winter of 2006 that horizontally there was a narrow transition zone, characterized by a thermocline and inverse halocline at 15 m WCD between the well-mixed coastal water (<25 m bottom depth) and shelf water (>60 m bottom depth). This transition zone was caused by downwelling and offshore transport of the low temperature and low salinity coastal water at the bottom and the shoreward transport of the higher temperature and salinity shelf water at the surface (Liu et al., 2010). However, the transition zone appears not a stable phenomenon as it was not observed in our winter cruise in 2009 (CHOICE-C winter cruise report: Cruise 2-China sea shelf systems, Xiamen University, 2010). Because site A9 is situated just in this transition zone, we tentatively attribute the cyclic pattern of TEX_{86}^{H} temperature curve at the site to the influence of the labile downwelling and offshore transport of coastal water. Apparently, more high resolution sedimentary records around the site are needed to examine this observation and its cause.

3.2. Mechanisms and implications

Our data show that there is a strong seasonal contrast in the TEX_{86}^{H}-based and $U_{37}^{K'}$-based sea water temperatures in the study area. Similar observations have been reported for, e.g. the Arabian Sea (Huguet et al., 2006) and Adriatic Sea (Leider et al., 2010), which were attributed to seasonal differences between the timing of the haptophyte and Thaumarchaeota blooms. Although haptophyte seasonal dynamics are not clear for the study area, algal blooms and maximal primary production have been found in summer when high fluvial nutrient influx occurs (Dai et al., 2008; Le et al., 2008; Song et al., 2010), which may be responsible for the spring-summer biased $U_{37}^{K'}$-based temperature in the sediments. Our winter biased TEX_{86}^{H} temperature is consistent with some previous observations showing that surface water Thaumarchaeota populations were abundant during winter and early spring in the Antarctic (Massana et al., 1998; Murray et al., 1998), the Arctic (Alonso-Sáez et al., 2008), the Adriatic Sea (Leider et al., 2010), near-shore waters off the island of Texel, The Netherlands (Wuchter et al., 2006) and the shallow, well-mixed southern North Sea (Herfort et al., 2007). The Thaumarchaeota decline with the onset of spring at these locations has been attributed to competition with bacteria that bloom in response to increased phytoplankton production (Massana et al., 1998; Murray et al., 1998; Church et al., 2003; Herfort et al., 2007), ensuing nutrient limitation (Wuchter et al., 2006; Herfort et al., 2007), or photoinhibition due to the increase in irradiance (Kalanetra et al., 2009). These scenarios occur similarly in our study area, i.e. during winter phytoplankton production declines in response to decreased terrestrial nutrient influx, and water column light levels are low due to the higher load of suspended particles caused by strong northeast monsoon-induced vertical mixing (Tang et al., 2007). These winter conditions are favorable for the bloom of Thaumarchaeota, and thus may be responsible for the winter biased TEX_{86}^{H} temperature.

Together with our previous observation that TEX_{86}^{H} reflected subsurface temperature in the open SCS (>300 m water depth; Jia et al., 2012), the finding of winter biased TEX_{86}^{H} temperature in coastal northern SCS suggests that there are two modes of Thaumarchaeota growth in the deep and shallow SCS, respectively. Although the two modes are spatially and temporally different, both show an inverse relationship with haptophyte growth, which might be caused by different responses of haptophyte and Thaumarchaeota to nutrient or light levels in the water column (e.g. Herfort et al., 2007; Kalanetra et al., 2009). Our results thus suggest that the application of both TEX_{86}^{H} and $U_{37}^{K'}$ gives different but complementary information on water temperature developments in past marine environments in the open and coastal SCS. Future studies on the seasonal abundance and community structure of haptophyte and Thaumarchaeota, as well as the distribution of

GDGTs, within the water column in the open and coastal SCS are required to better constrain the different organic proxies.

4. Conclusions

Temperature estimates from $U^{K'}_{37}$ and TEX^{H}_{86} proxies for five short sediment cores from the coastal northern South China Sea show that both proxies reflect temperature values that differ from annual mean WOA SST. Values based on $U^{K'}_{37}$ are higher than annual mean WOA SST and appear consistent with euphotic zone water temperature (0–30 m) in the spring and summer when fluvial nutrient influx and algal production are elevated. In contrast, values based on TEX^{H}_{86} are lower than annual mean WOA SST and exhibit a clear shoreward cooling trend, in agreement with winter SST distribution when nutrient and algal production declines. Our study suggests that each proxy may record different temperature signals (e.g. different season and water depth), highlighting the importance of constraining paleoproxies on regional scales for correct interpretation of reconstructed temperature.

Acknowledgements

We thank the expedition chief scientists, P. Cai and W. Zhai, and the crew of Dongfanghong II for support and help during the cruises. The cruise and laboratory studies were supported by the National Basic Research Program of China (2009CB421206) and by the National Natural Science Foundation of China (Nos. 41061160498 and 41276072). We are grateful to C. Zhang and an anonymous reviewer for valuable comments. This is contribution No. IS-1645 from GIGCAS.

Associate Editor—**S. Schouten**

References

Alonso-Sáez, L., Sánchez, O., Gasol, J.M., Balagué, V., Pedrós-Alio, C., 2008. Winter-to-summer changes in the composition and single-cell activity of near-surface Arctic prokaryotes. Environmental Microbiology 10, 2444–2454.

Castañeda, I.S., Schefuß, E., Pätzold, J., Sinninghe Damsté, J.S., Weldeab, S., Schouten, S., 2010. Millennial-scale sea surface temperature changes in the eastern Mediterranean (Nile River Delta region) over the last 27,000 years. Paleoceanography 25, PA1208. http://dx.doi.org/10.1029/2009PA001740.

Church, M.J., DeLong, E.F., Ducklow, H.W., Karner, M.B., Preston, C.M., Karl, D.M., 2003. Abundance and distribution of planktonic Archaea and Bacteria in the waters west of the Antarctic Peninsula. Limnology and Oceanography 48, 1893–1902.

Dai, M.H., Zhai, W.D., Cai, W.-J., Callahan, J., Huang, B.Q., Shang, S.L., Huang, T., Li, X.L., Lu, Z.M., Chen, W.F., Chen, Z.Z., 2008. Effects of an estuarine plume-associated bloom on the carbonate system in the lower reaches of the Pearl River estuary and the coastal zone of the northern South China Sea. Continental Shelf Research 28, 1416–1423.

Ge, H.M., Zhang, C.L., Dang, H.Y., Zhu, C., Jia, G.D., 2013. Distribution of tetraether lipids in surface sediments of the northern South China Sea: implications for TEX86 proxies. Geoscience Frontiers. 4, 223–229.

Herfort, L., Schouten, S., Boon, J.P., Sinninghe Damsté, J.S., 2006. Application of the TEX_{86} temperature proxy in the southern North Sea. Organic Geochemistry 37, 1715–1726.

Herfort, L., Schouten, S., Abbas, B., Veldhuis, M.J.W., Coolen, M.J.L., Wuchter, C., Boon, J.P., Herndl, G.J., Sinninghe Damsté, J.S., 2007. Variations in spatial and temporal distribution of Archaea in the North Sea in relation to environmental variables. FEMS Microbiology Ecology 62, 242–257.

Hopmans, E.C., Schouten, S., Pancost, R.D., Van der Meer, M.T.J., Sinninghe Damsté, J.S., 2000. Analysis of intact tetraether lipids in archaeal cell material and sediments by high performance liquid chromatography/atmospheric pressure chemical ionization mass spectrometry. Rapid Communications in Mass Spectrometry 14, 585–589.

Hopmans, E.C., Weijers, J.W.H., Schefuß, E., Herfort, L., Sinninghe Damsté, J.S., Schouten, S., 2004. A novel proxy for terrestrial organic matter in sediments based on branched and isoprenoid tetraether lipids. Earth and Planetary Science Letters 224, 107–116.

Huguet, C., Kim, J.-H., Sinninghe Damsté, J.S., Schouten, S., 2006. Reconstruction of sea surface temperature variations in the Arabian Sea over the last 23 kyr using organic proxies (TEX86 and $U^{K'}_{37}$. Paleoceanography 21, PA3003. http://dx.doi.org/10.1029/2005PA001215.

Huguet, C., Schimmelmann, A., Thunell, R., Lourens, L.J., Sinninghe Damsté, J.S., Schouten, S., 2007. A study of the TEX_{86} paleothermometer in the water column and sediments of the Santa Barbara Basin, California. Paleoceanography 22, PA3202. http://dx.doi.org/10.1029/2006PA001310.

Jia, G.D., Zhang, J., Chen, J.F., Peng, P.A., Zhang, C.L., 2012. Archaeal tetraether lipids record subsurface water temperature in the South China Sea. Organic Geochemistry 50, 68–77.

Jia, G.D., Xu, S.D., Chen, W.F., Lei, F., Bai, Y., Huh, C.-A., in press. 100-yr ecosystem history elucidated from inner shelf sediments off the Pearl River estuary, China. Marine Chemistry. http://dx.doi.org/10.1016/j.marchem.2013.02.005.

Kalanetra, K.M., Bano, N., Hollibaugh, J.T., 2009. Ammonia-oxidizing Archaea in the Arctic Ocean and Antarctic coastal waters. Environmental Microbiology 11, 2434–2445.

Kim, J.-H., Schouten, S., Hopmans, E.C., Donner, B., Sinninghe Damsté, J.S., 2008. Global sediment core-top calibration of the TEX_{86} paleothermometer in the ocean. Geochimica et Cosmochimica Acta 72, 1154–1173.

Kim, J.-H., van der Meer, J., Schouten, S., Helmke, P., Willmott, V., Sangiorgi, F., Koç, N., Hopmans, E.C., Sinninghe Damsté, J.S., 2010. New indices and calibrations derived from the distribution of crenarchaeal isoprenoid tetraether lipids: implications for past sea surface temperature reconstructions. Geochimica et Cosmochimica Acta 74, 4639–4654.

Kim, J.-H., Romero, O.E., Lohmann, G., Donner, B., Laepple, T., Haam, E., Sinninghe Damsté, J.S., 2012. Pronounced subsurface cooling of North Atlantic waters off Northwest Africa during Dansgaard–Oeschger interstadials. Earth and Planetary Science Letters 339–340, 95–102.

Le, F.F., Ning, X.R., Liu, C.G., Hao, Q., Cai, Y.M., 2008. Standing stock and production of phytoplankton in the northern South China Sea during winter of 2006. Acta Ecologica Sinica 28, 5775–5784 (in Chinese).

Le, F.F., Sun, J., Ning, X.R., Song, S.Q., Cai, Y.M., Liu, C.G., 2006. Phytoplankton in northern South China Sea in summer 2004. Oceanologia et Limnologia Sinica 37, 238–248 (in Chinese).

Lee, K.E., Kim, J.-H., Wilke, I., Helmke, P., Schouten, S., 2008. A study of the alkenone, TEX_{86}, and planktonic foraminifera in the Benguela Upwelling System: implications for past sea surface temperature estimates. Geochemistry Geophysics Geosystems 9, Q10019. http://dx.doi.org/10.1029/2008GC002056.

Lei, F., Li, Z.Y., Zhang, J., Chen, W.F., Jia, G.D., 2012. Sources and burial of organic carbon in coastal sediments off Guangdong Province during the past century. Journal of Tropical Oceanography 31, 62–66 (in Chinese).

Leider, A., Hinrichs, K.-U., Mollenhauer, G., Versteegh, G.J.M., 2010. Core-top calibration of the lipid-based $U^{K'}_{37}$ and TEX86 temperature proxies on the southern Italian shelf (SW Adriatic Sea, Gulf of Taranto). Earth and Planetary Science Letters 300, 112–124.

Liu, C.J., Xia, H.Y., Wang, D.X., 2010. The observation and analysis of eastern Guangdong coastal downwelling in the winter of 2006. Acta Oceanologica Sinica 32, 1–9 (in Chinese).

Lopes dos Santos, R.A., Prange, M., Castaneda, I.S., Schefuss, E., Mulitza, S., Schulz, M., Niedermeyer, E.M., Sinninghe Damsté, J.S., Schouten, S., 2010. Glacial–interglacial variability in Atlantic meridional overturning circulation and thermocline adjustments in the tropical North Atlantic. Earth and Planetary Science Letters 300, 407–414.

Massana, R., Taylor, L.T., Murray, A.E., Wu, K.Y., Jeffrey, W.H., DeLong, E.F., 1998. Vertical distribution and temporal variation of marine planktonic archaea in the Gerlache Strait, Antarctica, during early spring. Limnology and Oceanography 43, 607–617.

Murray, A.E., Preston, C.M., Massana, R., Taylor, L.T., Blakis, A., Wu, K., DeLong, E.F., 1998. Seasonal and spatial variability of bacterial and archaeal assemblages in the coastal waters near Anvers Island, Antarctica. Applied and Environmental Microbiology 64, 2585–2595.

Müller, P., Kirst, G., Ruhland, G., von Storch, I., Rosell-Melé, A., 1998. Calibration of the alkenone paleotemperature index $U^{K'}_{37}$ based on core-tops from the eastern South Atlantic and the global ocean (60°N–60°S). Geochimica et Cosmochimica Acta 62, 1757–1772.

Prahl, F.G., Wakeham, S.G., 1987. Calibration of unsaturation patterns in long-chain ketone compositions for paleotemperature assessment. Nature 330, 367–369.

Schouten, S., Hopmans, E.C., Schefuß, E., Sinninghe Damsté, J.S., 2002. Distributional variations in marine crenarchaeotal membrane lipids: a new organic proxy for reconstructing ancient sea water temperatures? Earth and Planetary Science Letters 204, 265–274.

Schouten, S., Hopmans, E.C., Sinninghe Damsté, J.S., 2013. The organic geochemistry of glycerol dialkyl glycerol tetraether lipids: a review. Organic Geochemistry 54, 19–61.

Song, X.Y., Liu, H.X., Huang, L.M., Tan, Y.H., Ke, Z.X., Zhou, L.B., 2010. Distribution characteristics of basic biological production and its influencing factors in the northern South China Sea in summer. Acta Ecologica Sinica 30, 6409–6417 (in Chinese).

Strong, D.J., Flecker, R., Valdes, P., Wilkinson, I.P., Rees, J.G., Zong, Y.Q., Lloyd, J.M., Garrett, E., Pancost, R.D., 2012. Organic matter distribution in the modern sediments of the Pearl River Estuary. Organic Geochemistry 49, 68–82.

Su, J.L., 2004. Overview of the South China Sea circulation and its influence on the coastal physical oceanography outside the Pearl River Estuary. Continental Shelf Research 24, 1745–1760.

Sun, J., Song, S.Q., Le, F.F., Wang, D., Dai, M.H., Ning, X.R., 2007. Phytoplankton in northern South China Sea in the winter of 2004. Acta Oceanologica Sinica 29, 312–345 (in Chinese).

Tang, S.L., Chen, C.Q., Zhan, H.G., Xu, D.Z., Liu, D.Z., 2007. Retrieval of euphotic layer depth of South China Sea by remote sensing. Journal of Tropical Oceanography 26, 9–15 (in Chinese).

Urakawa, H., Martens-Habbena, W., Stahl, D.A., 2010. High abundance of ammonia-oxidizing Archaea in coastal waters, determined using a modified DNA extraction method. Applied and Environmental Microbiology 76, 2129–2135.

Villanueva, J., Pelejero, C., Grimalt, J., 1997. Clean-up procedures for the unbiased estimation of C_{37} alkenone sea surface temperatures and terrigenous *n*-alkane inputs in paleoceanography. Journal of Chromatography 757, 145–151.

Wei, Y.L., Wang, J.X., Liu, J., Dong, L., Li, L., Wang, H., Wang, P., Zhao, M.X., Zhang, C.L., 2011. Spatial variations in archaeal lipids of surface water and core-top sediments in the South China Sea and their implications for paleoclimate studies. Applied and Environmental Microbiology 77, 7479–7489.

Weijers, J.W.H., Schouten, S., Spaargaren, O.C., Sinninghe Damsté, J.S., 2006. Occurrence and distribution of tetraether membrane lipids in soils: implications for the use of the TEX_{86} proxy and the BIT index. Organic Geochemistry 37, 1680–1693.

Wuchter, C., Abbas, B., Coolen, M.J.L., Herfort, L., van Bleijswijk, J., Timmers, P., Strous, M., Teira, E., Herndl, G.J., Middelburg, J.J., Schouten, S., Sinninghe Damsté, J.S., 2006. Archaeal nitrification in the ocean. Proceedings of the National Academy of Sciences of the USA 103, 12317–12322.

Zhai, W.D., Dai, M.H., Cai, W.-J., Wang, Y.C., Wang, Z.H., 2005. High partial pressure of CO_2 and its maintaining mechanism in a subtropical estuary: the Pearl River estuary, China. Marine Chemistry 93, 21–32.

Zhang, C.L., Wang, J., Wei, Y., Zhu, C., Huang, L., Dong, H., 2012. Production of branched tetraether lipids in the lower Pearl River and estuary: effects of extraction methods and impact on bGDGT proxies. Frontiers in Terrestrial Microbiology 2, 274. http://dx.doi.org/10.3389/fmicb.2011.00274.